PHYSICAL REVIEW B VOLUME 5, NUMBER 11 1 JUNE 1972

Canonical Distribution Law and KCl : Sm^{2+} Fluorescence: The C_{2v} Paradox*†

Richard H. Heist,‡ Charles R. Chilver, and Francis K. Fong§
Department of Chemistry, Purdue University, Lafayette, Indiana 47907
(Received 23 August 1971)

A combination of critical experiments has been carried out in order to elucidate the recent conclusions of Bradbury and Wong, who attributed all the dominant KCl : Sm^{2+} fluorescence lines to the nearest-neighbor $C_{2v}(1,1,0)Sm^{2+}-K^{+}$ vacancy site. In an extensive investigation into the radiationless quenching, characteristic lifetimes, excitation spectra, and Zeeman polarization of KCl : Sm^{2+} fluorescence lines, all the prominent lines are unequivocally attributed to a distribution of three different $Sm^{2+}-K^{+}$ vacancy sites. In addition, 18 weak lines are shown to originate from dimeric cluster and O^{2-} compensated sites. The paradoxical C_{2v} interpretations of Bradbury and Wong are shown to be based on incorrect premises, inadequate experimentation, and confusion in the identity of samples with different dopant concentrations.

I. INTRODUCTION

This paper deals with and resolves the conflicting interpretations which exist in the literature on the line-fluorescence spectrum of the KCl : Sm^{2+} system. The basic problem involves the question whether the dominant lines of KCl : Sm^{2+} fluorescence arise from a single $C_{2v}(1,1,0)$ $Sm^{2+}-K^{+}$ vacancy pair, i.e., the nearest-neighbor pair, or from a distribution of pairs, as one might expect from statistical-mechanical considerations. Since the problem is immediately related to the general problem of ion-defect interactions in lattices in which substitutional aliovalent cations are charge compensated by intrinsic defects, a brief but comprehensive review of the development of investigations on compensated lattices appears appropriate. Such a review is given in Sec. II. In Sec. III, the conflicting interpretations of the KCl : Sm^{2+} fluorescence are summarized. In order to resolve the conflicting views, four sets of critical experiments have been chosen: measurements of (a) the temperature dependence of the radiationless quenching, (b) the radiative relaxation times, (c) the excitation spectra, and (d) the Zeeman polarization of the KCl : Sm^{2+} fluorescence lines. The experimental procedures and results are described in Secs. IV and V, respectively. The interpretations of the results and the detailed spectroscopic assignments are presented in Sec. VI. The results show unequivocally that the prominent KCl : Sm^{2+} fluorescence lines arise from three different sites corresponding to the $C_{4v}(2,0,0)$, $C_{2v}(1,1,0)$, and $C_s(2,1,1)$ $Sm^{2+}-K^{+}$ vacancy pairs. In Sec. VII, 18 weak lines are attributed to dimeric cluster and O^{2-} compensated sites.

II. ION-DEFECT INTERACTION IN COMPENSATED LATTICES

Recently, the problem of the compensated lattice has been likened to that of unipositive cations and anions interacting in a periodic lattice.[1-5] The problem of impurity ion-defect pair formation in alkali halides[1,3-5] and alkaline earth halides[2] doped with divalent and trivalent cations has been treated in terms of canonical partition functions. At elevated temperatures, complete dissociation of the ion-defect pairs occurs, and the description is one of weakly interacting ions in a quasirandom distribution.[3,4] At low temperatures, at which the interaction energies are large compared to the average thermal energy, the ions and their compensation defects form pairs in a statistical distribution of various site symmetries consistent with the geometric restrictions of the lattice.[1-3] In the intermediate-temperature region in which neither of the above descriptions is valid, the problem is treated in the notion of an equilibrium mixture of a distribution of ion-defect pairs and ions and defects in approximately random distribution.[4,5] The statistical-mechanical treatment of ion-defect interactions has also been extended to the formation of dimeric and trimeric clusters at varying temperatures and concentrations.[6]

The problem of site multiplicity in alkali-halide : divalent-cation systems has been investigated by a large number of workers. Numerous studies on the broadening of the Debye loss curve observed for the dielectric relaxation of divalent-cation–vacancy pairs suggest the presence of inequivalent dipolar pairs.[7-13] Franklin and co-workers,[12,13] in particular, have considered the contribution of the $C_{2v}(1,1,0)$, $C_{4v}(2,0,0)$, and $C_s(2,1,1)$ pairs to dielectric relaxation. Although early theories[14-17] on the conductivity of alkali-halide : divalent-cation crystals have been formulated on the assumption that only the nearest-neighbor pairs are bound, the notion of the association and dissociation of the bound pairs in ionic conductivity suggests the varying degree of association of the vacancies with the divalent cations. In electron-spin-resonance ex-

periments, Watkins[18,19] observed for several alkali-halide : Mn^{2+} systems signals corresponding to the $C_{2v}(1, 1, 0)$, $C_{4v}(2, 0, 0)$ Mn^{2+} vacancy pairs, a more distant pair which was attributed to a "cubic" site, and a second C_{4v} site presumably arising from divalent-anion (such as O^{2-}) impurity compensation.

In addition to the multiplicity of divalent-cation sites arising from vacancy compensation, there is considerable evidence for the clustering of ion-defect pairs in alkali halides doped with divalent cations.[18-26] While the nature of the clusters is not quite as well known as that of ion-defect pairs it has been established by a number of investigators[18-26] that it is possible to eliminate the presence of clusters (as well as the O^{2-} compensated sites[26]) by means of the rapid quenching of crystals annealed at elevated temperatures.

In the statistical-mechanical treatment of the compensated lattices by Fong and co-workers,[1-6] numerical calculations of the site distribution arising from vacancy compensation and cluster formation have been made and compared to experimental observations. While the quantitative aspects of these calculations are limited by the accuracies of the values (taken from earlier theoretical[27-30] and experimental[18,19] investigations) assumed for the interaction energies, the true significance of the results of these calculations lies in the unification of a large number of observations into one single framework of well-founded first principles.

III. CONFLICTING INTERPRETATIONS OF KCl : Sm^{2+} FLUORESCENCE

The KCl : Sm^{2+} system plays an important role in the study of charge compensations in view of its unique optical properties. The fluorescence spectrum of the KCl : Sm^{2+} system is probably one of the most frequently investigated spectra in recent years.[25,26,31-46] The first detailed investigation on KCl : Sm^{2+} fluorescence was made by Bron and Heller,[31] who interpreted all the dominant fluorescence lines in terms of the single $C_{2v}(1, 1, 0)$ Sm^{2+} – K^+ vacancy pair. Fong and Wong[32,33] pointed out the possibility of the Sm^{2+} ion being compensated by a K^+ vacancy along crystal axes other than the [110] axis. These authors proved the existence of tetragonal Sm^{2+}-ion sites by the observation of C_{4v} Zeeman anisotropy fluorescence (ZAF) patterns in prominent $^5D_0 \rightarrow {}^7F_4$ and $^7F_6$ lines.[32,33,36] The importance of Sm^{2+}-K^+ vacancy pairs other than the nearest-neighbor $C_{2v}(1, 1, 0)$ pairs was further suggested by the work of Buchanan and Woll,[34] who assumed that the compensation vacancy is sufficiently distant and that noncubic distortions about the Sm^{2+} ion can be neglected in arriving at a qualitatively good theoretical fit of the vibronic sidebands of Sm^{2+} in KCl and KBr.

Since the Sm^{2+} (ionic radius = 1.12 Å) and the Sr^{2+} (ionic radius = 1.13 Å) ions are practically identical in size,[47] the site-distribution calculations based on the interaction energies of the KCl : Sr^{2+} system should at least give a qualitative description of what might be expected of the site distribution in the KCl : Sm^{2+} system. On the basis of this expectation, a dominant line in the $^5D_0 \rightarrow {}^7F_3$ transition was attributed to the third-nearest-neighbor $C_s(2, 1, 1)$ site. It was noted[37] that (since the ion-defect interaction energies in the KCl : Mn^{2+} system were found[18,19] to be in agreement with those calculated[28,29] for the KCl : Sr^{2+} system) the observation of the third-nearest-neighbor $C_s(2, 1, 1)$ site in KCl : Sm^{2+} would be compatible with the electron-spin-resonance observation of the cubic Mn^{2+} site by Watkins.[18,19] The original C_s assignment[37] appeared to be incorrect, however, since it did not account for all the observed points, and the ZAF patterns were redetermined by Fong, Sundberg, Heist, and Chilver,[41] who ascertained the origins of two overlapping ZAF patterns by means of field-dependence data and greatly improved plate-reading techniques. The result confirmed the presence of the $C_s(2, 1, 1)$ site as well as indicated the observation of a hitherto unobserved C_{3v} ZAF pattern.[41]

All the ZAF investigations described above have been carried out at fields up to 27 kG, at which measurable Zeeman effects are observed only for $^5D_0 \rightarrow {}^7F_J$ transitions with $J \geq 3$. Fong and Bellows[40] employed magnetic fields up to 93.5 kG in an investigation of the ZAF patterns of the low-J ($^5D_0 \rightarrow {}^7F_0$, $^7F_1$, and $^7F_2$) transitions. At 93.5 kG, all the 23 observed fluorescence lines arising from the low-J transitions show Zeeman effects, 11 of which give rise to ZAF patterns which were attributed to C_{2v}, C_{4v}, and C_s origins.[40]

While the Zeeman studies of Fong and co-workers[32,33,36-38,40,41] appeared to have firmly established the multisite origin of the KCl : Sm^{2+} fluorescence lines, Bradbury and Wong[43-46] refuted all the non-C_{2v} symmetry assignments of the prominent lines made from ZAF studies (including the original discovery by Fong and Wong[32,33] of the C_{4v} origin of several important lines in $^5D_0 \rightarrow {}^7F_4$ and $^7F_6$ transitions), as they claimed that all the prominent lines originate from the $C_{2v}(1, 1, 0)$ site. The major conclusions of these authors are (a) The ZAF patterns arising from the $^5D_0 \rightarrow {}^7F_3$ 7693.5- and 7694.5-Å zero-field lines both originate from the same Sm^{2+} ion of C_{2v} origin.[44] (b) All the prominent lines in the low-J (≤ 2) transitions originate from the same C_{2v} Sm^{2+} ion.[45] (c) From the temperature dependence of fluorescence intensities and lifetimes, all the prominent lines can be attributed to a single C_{2v} Sm^{2+} site. Two sets of much weaker

lines may be attributed to the more distant pairs.[45] (d) The well-resolved first-order C_{4v} patterns observed by Fong and Wong[33] in $^5D_0 \rightarrow {}^7F_4$ and $^7F_6$ transitions are in fact second-order C_{2v} patterns.[45] (e) The differences in the spectroscopic properties of the so-called type-I and type-II crystals are due to aging effects in the type-II crystals.[46] The $Sm^{2+} - K^+$ vacancy system does not reach thermodynamic equilibrium at room temperature, at least in "a couple of years."

Conclusion (e) was based on the fact that two different types (I and II) of $KCl:Sm^{2+}$ crystals display different relative populations of three major groups of lines, and that more lines were observed in the type-II samples. Type-I crystals were grown at UCLA. Type-II crystals were incorrectly stated by Bradbury and Wong as those used by Fong and Wong[33] a few years ago in their original ZAF work on $KCl:Sm^{2+}$. The crystal employed in the Fong and Wong work, containing 3.2×10^{18} Sm^{2+}-ions cm^{-3} (see Sec. III of Fong and Wong[33]), was the lowest in dopant concentration of four Sm^{2+} concentrations grown in Fong's laboratory in 1965. The other three Sm^{2+}-ion concentrations were 1.4×10^{19}, 3.5×10^{19}, and 5.1×10^{19} cm^{-3}. The details of the crystal growth and the methods of quantitative analysis of the Sm^{2+} content were given in Fong, Cape, and Wong.[48] The fluorescence spectra of the more concentrated crystals give rise to a large number of new lines as reported by Fong, Heist, Chilver, Bellows, and Ford.[36] The type-II spectrum displayed by Bradbury and Wong[46] corresponds to the samples containing 3.5×10^{19} Sm^{2+}-ions cm^{-3} (Sec. VII). The type-I spectrum of Bradbury and Wong is identical to the original Fong and Wong spectrum of the low-concentration sample [compare, for example, Fig. 2(a) of Bradbury and Wong[45] and Fig. 6 of Fong and Wong[33]]. The type-I spectrum measured by Fong and Wong in 1965 has been reproduced, *on the same crystal*, by Fong and Bellows in 1969, Fong, Sundberg, Heist, and Chilver[41] in 1970, and the present authors in 1971. The mistake in sample identification was apparently responsible directly or indirectly for all the premises which led Bradbury and Wong to the erroneous conclusions listed in items (a)–(e).

Conclusions (a)–(d) of Bradbury and Wong are refuted in Secs. IV–VII of the present paper, as the proper symmetry assignments are established through the interpretations of a combination of crucial experimental results. Many of the techniques employed by the present authors were not available to Bradbury and Wong. Important among these are (i) much more intense pump sources, (ii) high-resolution microdensitometer comparator, (iii) magnetic fields in excess of 90 kG, (iv) phase-sensitive detection, (v) analog-to-digital conversion, and (vi) multi- (1000) channel signal averaging.

IV. EXPERIMENTAL PROCEDURE

Single-crystalline $KCl:Sm^{2+}$ samples originally grown and analyzed in the manner described by Fong, Cape, and Wong[48] are employed in the present work. The rare-earth concentrations are in the range 10^{18}–10^{20} ions cm^{-3}.[48] The radiationless quenching and lifetime measurements were made on a 2-m Jarrell-Ash Czerny-Turner spectrograph with a resolving power of 120 360 and a grating blazed at 1 μ. The excitation spectra were measured on a 0.5-m Jarrell-Ash Ebert monochrometer with a resolving power of 61 360 and a 0.5-μ-blazed grating. The slitwidths of the 0.5-m spectrometer employed in the excitation experiments ranged from 100–200 μ, depending on the fluorescence intensity. The scanning monochrometer was a 0.25-m Jarrell-Ash Ebert monochrometer with a resolving power of 72 520 and a 0.6-μ-blazed grating. The 0.25-m slitwidth was held constant at 500 μ, and the grating was scanned at 16.2 Å/min. A 900-W Osram Xe-arc lamp was used as the light source for the thermal-quenching experiments and excitation spectra. The source for the lifetime measurements was an EGG FX-12 flashlamp with a 1-W-power output. All spectra were taken photoelectrically using RCA photomultiplier tubes with S-20 or S-1 response, depending upon the spectral region of interest. Red No. 2030 and blue No. 9780 Corning filters were used except for the excitation experiments, where no blue filter was used.

Phase-sensitive detection techniques were used for the excitation spectra. The sample fluorescence was chopped by a frequency-controlled motor accurate to 0.5%. The output of the photomultiplier was fed into a phase-sensitive detection system consisting of a Keithly nanovolt amplifier, a Keithly phase shifter, and a Keithly phase-sensitive detector. The resulting signal was displayed on a strip-chart recorder. For the radiationless quenching experiments, phase-sensitive detection techniques were used in conjunction with the S-1 photomultiplier tube in measuring $^5D_0 \rightarrow {}^7F_5$ and $^7F_6$ fluorescence lines. For $^5D_0 \rightarrow {}^7F_J$ $(0 \leq J \leq 4)$ lines, a current-voltage converter with a range of 10^{-7} to 10^{-10} A/V and a multirange active filter built at Purdue (serving as a variable damping device using an operational amplifier) was used with the S-20 photomultiplier tube. In each case, the final output was displayed on a strip-chart recorder.

The output from the photomultiplier tube for the lifetime measurements was monitored on a Techtronix scope. The vertical output from the scope was converted to digital form, and multi- (1000) channel signal averaged with a PDP 8/L computer.

A number (N) of trials was made on each line. The number of flashes per trial ranged from 225 to 8000, depending upon the apparent signal-to-noise ratio. The lifetime was then determined from a reiterative least-squares computer fit of an exponential decay to the multichannel averaged data. Convergence was achieved when the sums of squares of the differences between the exponential fit and the experimental data was at a minimum. The slitwidth of the spectrograph was an important factor, especially for measuring the lifetimes of closely spaced lines. Care was taken to ensure the necessary resolution. The change in fluorescence intensity as a function of temperature was ascertained by the integration of the area under the recorder trace, and by measurement of the changes in the peak height.

The temperature-variation apparatus built at Purdue after the design of Welber and Tynan[49] for the thermal-quenching experiments consisted of a variable-voltage source used to heat a copper-sample holder wound with nichrome heater wire. The sample holder was insulated from the helium bath by a Teflon block and a cotton plug. The temperature of the sample holder was monitored using a carbon resistor mounted in the holder. Temperatures up to 65 K were attained with this device, although the helium-boil-off rate increased markedly above 40 K.

By means of the procedure outlined above, it is possible to ascertain lifetimes reproducible to within 0.4% for strong signals. For weaker signals, the lifetime measurements are reproducible to within 2%. In contrast to the computer-averaging procedure employed by the present authors, an unspecified number of scope traces were photographed to provide a photographic average in the Bradbury-Wong experiment, and each photo was reduced by hand on a semilog plot to determine the decay time.[46]

The high intensity of the 900-W Xe-arc lamp (compared to the 100-W tungsten lamp in the Bradbury-Wong experiment) makes possible the determination of the temperature dependence of line intensities of the higher-J transitions as well as the excitation spectra of several weak lines with thermal-quenching behavior different from that of the prominent lines. The 7022.7-, 7258.0-, and 7282.8-Å excitation spectra were measured with a 10-sec time constant because of small signal-to-noise ratios. The 7014.7-Å excitation spectra was measured using a 0.3-sec time constant.

High-field measurements were made at the Francis Bitter National Magnet Laboratory employing a 2-m Bausch and Lomb grating spectrograph. Reading of the photoplates was accomplished by means of a direct-scanning Grant-Daytex microdensitometer comparator which was coupled to a Varian Statos I (model 150) electrostatic recorder. The comparator has a reproducibility of $\pm 0.25\ \mu$ and is equipped with both a viewing screen and a split-image–oscilloscope display which enhances speed and accuracy of photoplate alignment. A photomultiplier takes transmittance (T) data and presents it as a $(1-T)$ density value. Reproducibility was in most cases better than 0.05 Å.

The high-temperature annealing-quenching experiments were performed in 8-mm quartz tubes after the procedure of Fenn, Cox, and Fong.[26]

V. EXPERIMENTAL RESULTS AND INTERPRETATIONS

A. Radiationless Thermal Quenching

The temperature dependence of 39 lines in the fluorescence spectrum of KCl : Sm^{2+}, corresponding to the relaxation of Sm^{2+} from $^5D_0$ to all the seven J (0–6) multiplets of the ^7F term, has been determined. The results are displayed in Figs. 1–3. It is found that the thermal-quenching characteristics of all the fluorescence lines measured fall into one of three categories with the radiationless quenching process becoming significant at (a) 15 K, (b) 20 K, and (c) 27 K, respectively. All the dominant KCl : Sm^{2+} fluorescence lines appear to belong to group (a) while the weaker lines belong to groups (b) and (c). The lines in groups (b) and (c) disappear when the samples are quenched from elevated temperatures without apparently affecting the intensities of the group-(a) lines. This effect is shown in Figs. 4 and 5 for the $^5D_0 - {}^7F_0$ and $^7F_1$ transitions, respectively. At room temperature, the missing lines of the quenched samples reappear in approximately two weeks. Details of the high-temperature annealing experiments under various controlled atmospheres are given elsewhere.[26] The intensity-quenching process is intimately related to the lifetime quenching of KCl : Sm^{2+} first reported by Baldini, Cartoceti, and Guzzi.[42] Both phenomena can be explained in terms of a nearby level which thermally depopulates the emitting $^5D_0$ level. Treating this model as a three-level system, the resulting solution to the corresponding steady-state rate equations gives the expression for the temperature-dependent fluorescence intensity

$$I(T)/I_0 = (\alpha e^{-\Delta E/kT} + \beta)^{-1} \ , \qquad (1)$$

where $I(T)$ and I_0 are the fluorescence intensities at temperature T and $T = 0$ K, respectively, α is a constant characteristic of the onset of thermal quenching, and β is normalized to unity for all cases. The solid curves in Figs. 1–3 are plots of Eq. (1) with (a) $\Delta E = 122.3\ \mathrm{cm}^{-1}$, $\alpha = 13\,106.9$; (b) $\Delta E = 162.2\ \mathrm{cm}^{-1}$, $\alpha = 5934.4$; and (c) $\Delta E = 209.9$

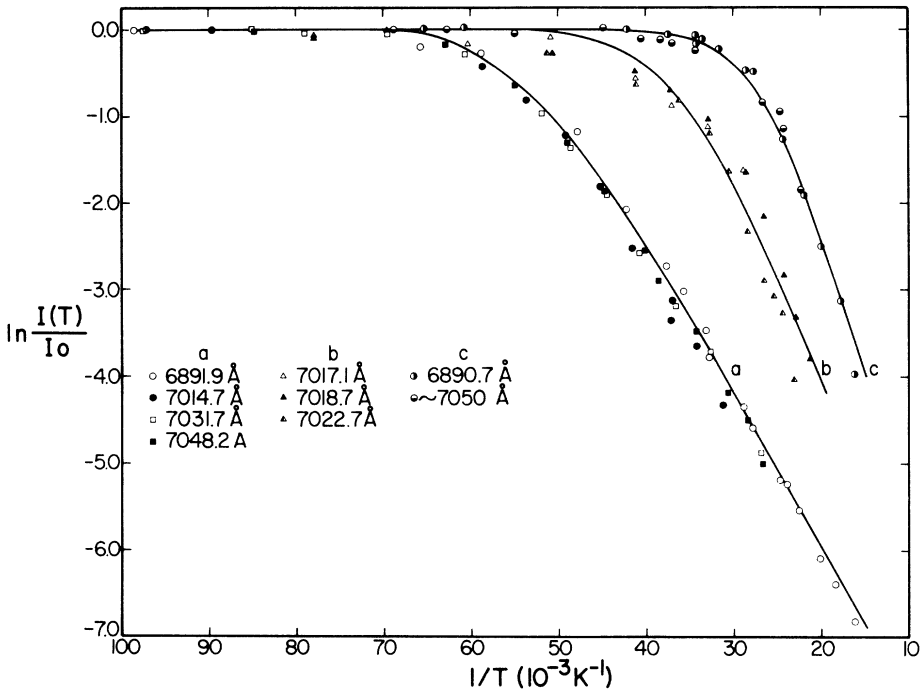

FIG. 1. Temperature dependence of the fluorescence intensity for KCl : Sm^{2+} $^5D_0 \rightarrow {}^7F_0$ and $^7F_1$ transitions. The solid curves are theoretical plots calculated from Eq. (1) with (a) $\Delta E = 122.3$ cm^{-1}, $\alpha = 13\,106.9$; (b) $\Delta E = 162.2$ cm^{-1}, $\alpha = 5934.4$; and (c) $\Delta E = 209.9$ cm^{-1}, $\alpha = 4506.9$.

cm^{-1}, $\alpha = 4506.9$. The temperature dependence for the lines in the 8746–9440-Å-wavelength region ($^5D_0 \rightarrow {}^7F_5$ and $^7F_6$) was measured using a photomultiplier tube with a S-1 response. The signal-to-noise ratio was several times smaller than that for the S-20 photomultiplier tube employed for the rest of

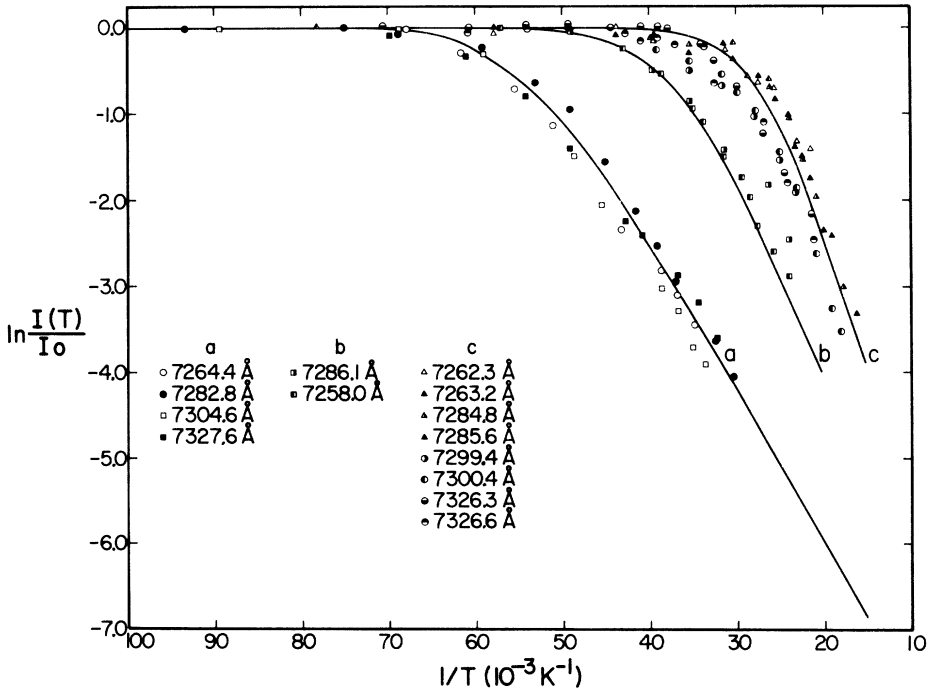

FIG. 2. Temperature dependence of the fluorescence intensity for KCl:Sm^{2+} $^5D_0 \rightarrow {}^7F_2$ transitions. The solid curves were calculated from Eq. (1) with the same parameters given in Fig. 1.

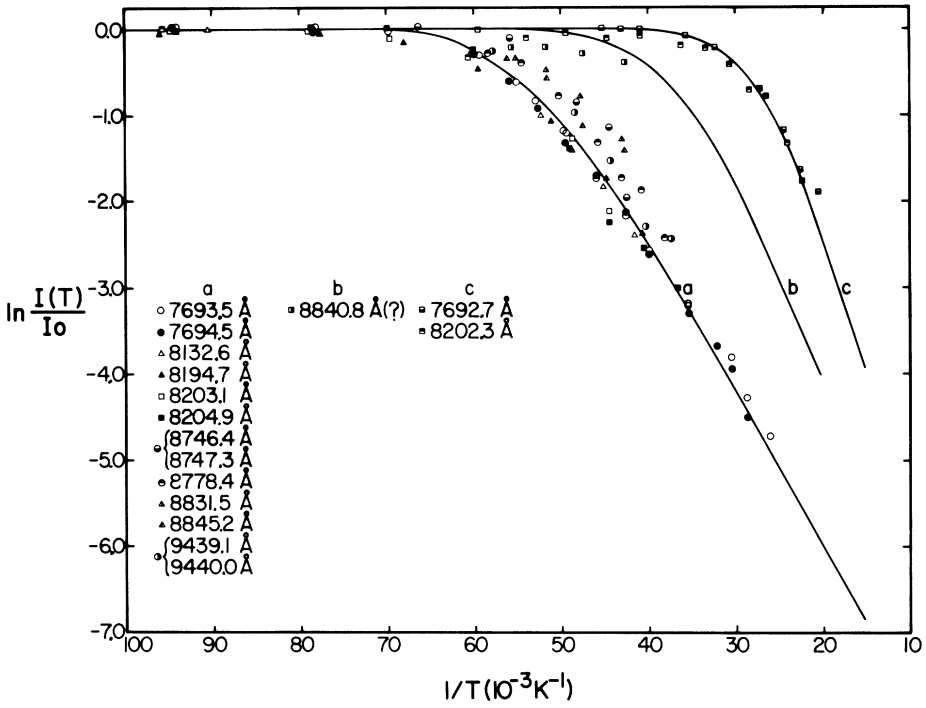

FIG. 3. Temperature dependence of the fluorescence intensity for KCl : Sm^{2+} $^5D_0 \rightarrow {}^7F_3$, $^7F_4$, $^7F_5$, and $^7F_6$ transitions. The solid curves were calculated from Eq. (1) with the same parameters given in Fig. 1.

the ^7F_J levels, resulting in the larger scatter in the data points shown in Fig. 3. The quenching studies also revealed the presence of a number of lines that are normally hidden by stronger lines at lower temperatures. For example, the lines at 7050, 7692.7, and 8840.8 Å are all totally or partially hidden by the stronger lines at 7048.2, 7693.5, and 8845.2 Å, respectively.

B. Characteristic Radiative Lifetimes

The 4.2-K lifetimes measured for $^5D_0 \rightarrow {}^7F_J$ ($J \leq 4$) transitions are listed in Table I along with the standard deviation, number of trials N, number of flashes per trial, slitwidth, relative intensity, temperature dependence, and the best site-symmetry assignments made in Sec. VI. The results listed in Table I indicate that the group-(a) fluorescence lines exhibit two *distinctly different* sets of lifetime values. The lines at 7282.8 Å ($^5D_0 \rightarrow {}^7F_2$), 7694.5 Å ($^5D_0 \rightarrow {}^7F_3$), 8132.6 Å ($^5D_0 \rightarrow {}^7F_4$), and 8194.7 Å ($^5D_0 \rightarrow {}^7F_4$) have lifetimes ranging from 10.5 to 10.66 msec. The remaining group-(a) lines have lifetimes ranging from 10.83 to 11.01 msec. Similarly to group-(b) lines, the 7258.0 Å ($^5D_0 \rightarrow {}^7F_2$) line has a lifetime of 9.57 msec, while the remainder of the lifetimes range from 7.60 to 7.98 msec.

C. Excitation Spectra, Zeeman Polarization, and Concentration Dependence

The excitation spectra of four KCl : Sm^{2+} fluorescence lines are shown in Figs. 6–8. In Fig. 6, the 4.2-K excitation spectrum of the 7014.7-Å line and the KCl : Sm^{2+} absorption spectrum are compared. The excitation spectra of the 7014.7-Å ($^5D_0 \rightarrow {}^7F_1$), 7022.7-Å ($^5D_0 \rightarrow {}^7F_1$), 7258.0-Å ($^5D_0 \rightarrow {}^7F_2$), and 7282.8-Å ($^5D_0 \rightarrow {}^7F_2$) lines are shown in Figs. 7 and 8. The similarity in the gross features of the excitation spectra for the 7014.7- and the 7282.8-Å line is noted (Fig. 7). This similarity is consistent with the similarity in the lifetimes (Sec. V B) and in the temperature dependence of the radiationless quenching of all the group-(a) lines.

The fluorescence lines in group (b) were found to exhibit thermal properties distinctly different from those of the group-(a) lines. This difference is reflected in their excitation spectra (Fig. 8). The 7258.0- and the 7022.7-Å-excitation spectra peak approximately 80 and 235 cm^{-1}, respectively, to the high-energy side of the 7014.7-Å-excitation spectrum. No excitation spectra were measured for the group-(c) lines because of their unfavorable signal-to-noise ratios.

The polarization assignments for the 46.6- and

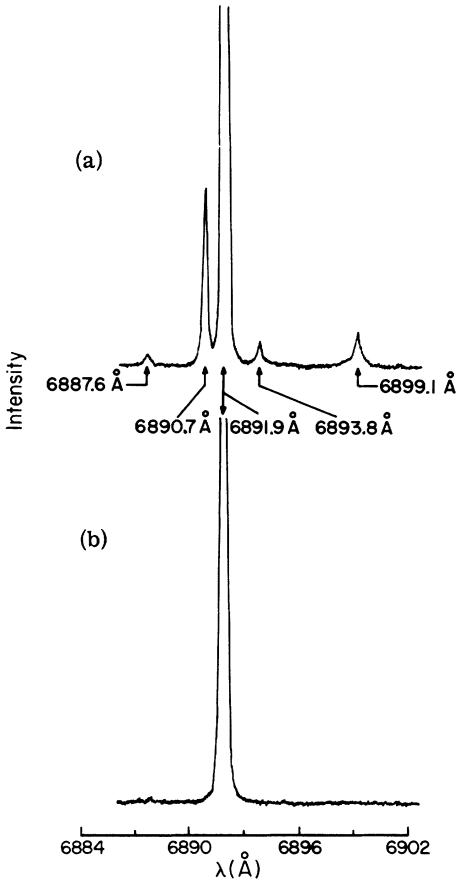

FIG. 4. Comparison of 4.2-K fluorescence spectra of KCl : Sm^{2+} samples before and after high-temperature annealing quenching: (a) $^5D_0 \rightarrow {}^7F_0$ lines of the original sample before annealing; (b) $^5D_0 \rightarrow {}^7F_0$ lines of the same sample after it was quenched from annealing at 650 °C and 5×10^{-5} Torr. At room temperature, sample (b) reverts to sample (a) with a half-life of approximately two weeks.

93.5-kG Zeeman components of the two prominent $^5D_0 \rightarrow {}^7F_3$ 7693.5- and 7694.5-Å zero-field lines are given in Fig. 9. The 7691.4- and 7695.1-Å components in Fig. 9 originate from the 7694.5-Å zero-field line. The 7693.3-Å component in Fig. 9 arises from the 7693.5-Å zero-field line. The 7689.0- and 7695.8-Å components in Fig. 10 originate from the 7694.5-Å zero-field line, while the 7692.4- and 7692.8-Å components originate on the 7693.5-Å zero-field line. The concentration dependence of the $^5D_0 \rightarrow {}^7F_4$ fluorescence is shown in Fig. 11. All spectral lines discussed elsewhere in the paper correspond to 3.2×10^{18}-cm^{-3} concentration.

VI. SYMMETRY DISTRIBUTION AS REVEALED BY GROUP-(a) LINES

In Sec. V B, distinctly different sets of lifetimes have been observed for a single group of lines having apparently the same temperature dependence. Since lines of the same site origin must have the same characteristic lifetime,[39,41] we conclude that any two fluorescence lines which have the same apparent temperature dependence *do not necessarily originate from the same site*, contrary to the premise upon which conclusion (c) of Bradbury and Wong (Sec. III) was based.

When the sample is quenched from elevated temperatures, only the group-(a) lines apparently remain unchanged (Figs. 4 and 5). In KCl : Sm^{2+}, charge compensation is predominantly provided for by K^+ cation vacancies if the lattice is free of divalent-anion impurities such as O^{2-} ions. Cation-vacancy motion in alkali halides has been investigated by a number of workers.[15,18,19,50] The time required for the thermal equilibration of isolated divalent cations with K^+ vacancies in KCl at temperature T is on the order of[26,50]

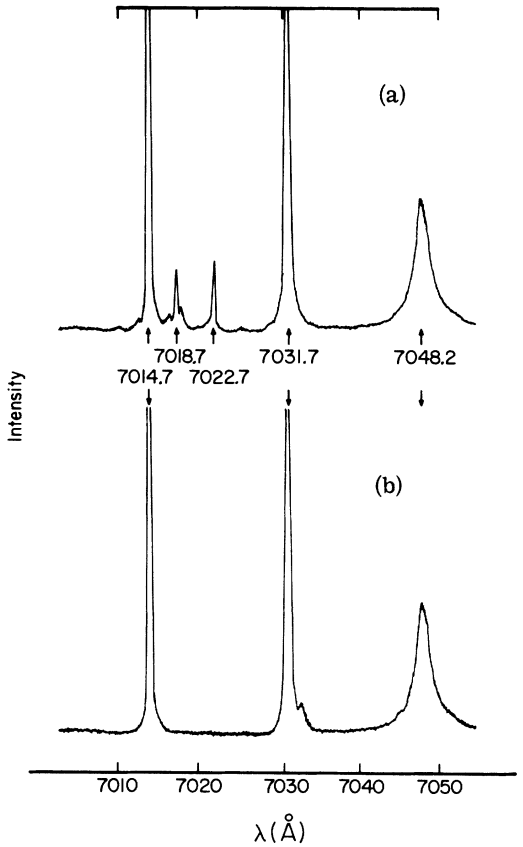

FIG. 5. Comparison of 4.2-K fluorescence spectra of KCl : Sm^{2+} samples before and after high-temperature annealing quenching: (a) $^5D_0 \rightarrow {}^7F_1$ lines of the original sample before annealing; (b) $^5D_0 \rightarrow {}^7F_1$ lines of the same sample after it was quenched from annealing at 650 °C and 5×10^{-5} torr.

TABLE I. Temperature dependence, 4.2-K lifetime measurements, and relative intensity values of the 39 observed fluorescence lines in KCl : Sm^{2+}. The standard deviations, number of trials N, number of flashes per trial, and slitwidths refer to the lifetime measurements. The best symmetry assignment, representation origin, and dipole origin (m, magnetic dipole; e, electric dipole) are also listed.

Transition	λ (Å)	Temperature dependence	4.2-K lifetime (msec)	Standard deviation	Number of trials (N)	Number of flashes per trial	Slitwidth (μ)	Relative intensity[a]	Best symmetry assignment (dipole origin)
$^5D_0 \rightarrow {}^7F_0$	6887.6		9.22		1	2000	100		
	6890.7	c	7.60	±0.13	4	1000	100	1.6	
	6891.9	a	10.89	±0.06	4	500	100	10.00	$C_{2v}, A_1(e)$
	6893.8		5.80		1	2000	100		
	6899.1		<50 μsec						
$^5D_0 \rightarrow {}^7F_1$	7014.7	a	10.93	±0.04	4	500	100	9.1	$C_{2v}, B_1(m)$
	7017.1	b							
	7018.0	b	7.98		1	400	100	0.6	
	7022.7	b	7.77	±0.08	4	1000	100	0.7	
	7031.7	a	10.93[b]	±0.11	3	500	100	9.3	C_{2v}, A_2 or $B_2(m)$
	7048.2	a	10.83	±0.06	4	500	100	9.3	C_{2v}, B_2 or $A_2(m)$
	7050.0	c							
$^5D_0 \rightarrow {}^7F_2$	7258.0	b	9.57		1	1000	100	0.3	
	7262.3	c							
	7263.2	c	7.80	±0.04	3	1000	100	0.4	
	7264.4	a	10.83		1	225	100	7.2	$C_{2v}, A_1(e)$
	7282.8	a	10.65	±0.03	3	500	100	1.0	$C_s, A'', (e)$
	7284.8	c	7.84	±0.03	4	1000	100	0.4	
	7285.6	c							
	7286.1	b							
	7299.4	c							
	7300.9	c	7.94	±0.07	4	1000	100	0.6	
	7304.6	a	10.89	±0.09	4	500	100	5.2	$C_{2v}, B_2(e)$
	7326.3	c							
	7326.6	c							
	7327.6	a	10.89[b]	±0.08	4	500	100	7.4	C_{2v}, A_1 or $B_1(e)$
$^5D_0 \rightarrow {}^7F_3$	7692.7	c							
	7693.5	a	11.01	±0.08	4	2000	30	6.4	C_{2v}, A_1 or $B_1(e)$
	7694.5	a	10.66	±0.17	3	4000–8000	30	3.1	$C_s, A'(m)$
$^5D_0 \rightarrow {}^7F_4$	8132.6	a	10.54	±0.16	4	1000	280	6.9	$C_{4v}, A_1(e)$
	8194.7	a	10.51		1	500	140	16.9	$C_{4v}, E(e)$ or $A_1, A_2(m)$
	8202.3	c						9.6	
	8203.1	a						12.6	
	8204.9	a	11.01	±0.11	4	500	100	56.5	C_{2v}, A_1 or $B_1(e)$
$^5D_0 \rightarrow {}^7F_5$	8746.4	a						11.5[c]	C_{2v}
	8747.3	a							C_{2v}
	8778.4	a						25.5	
	8831.5	a						34.8	
	8840.8	b							
	8845.2	a						26.2	
$^5D_0 \rightarrow {}^7F_6$	9439.1	a						42.9[c]	C_{4v}, A_1 or $A_2(m)$
	9440.0	a							C_{4v}, A_2 or $A_1(m)$
	9451.9								
	9503.3							2.8	
	9515.0							1.8	
	9522.5							4.7	

[a]Relative intensities were corrected for photomultiplier quantum efficiency and grating efficiency. The slitwidths used were 30μ for all transitions except $^5D_0 \rightarrow {}^7F_5$, $^7F_6$, where 500-μ slitwidths were used.

[b]Taken with a 0.25-m monochrometer.

[c]These lines could not be resolved so the total intensity is given.

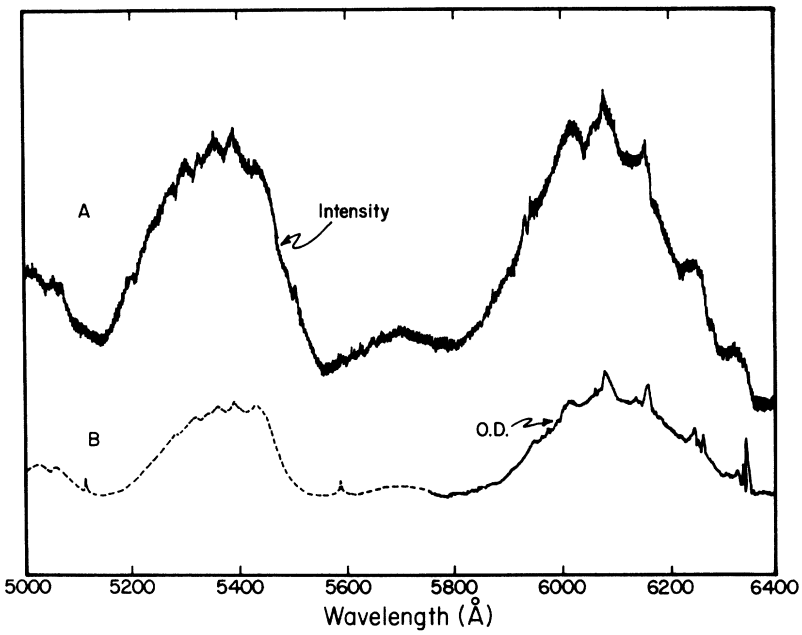

FIG. 6. Comparison of (a) 4.2-K excitation spectrum of the 7014.7 Å ($^5D_0 \rightarrow {}^7F_1$), and (b) 4.2-K absorption spectrum of KCl : Sm^{2+}. [The part of spectrum in dashed lines is taken from the 10-K measurement of Bron and Heller (Ref. 31).] O.D. represents optical density.

$$\tau = 10^{-14} e^{+0.9\,\mathrm{eV}/kT} , \qquad (2)$$

from which we obtain $\tau \sim 10$ and $\sim 10^{-5}$ sec at $T = 300$ and 500 K, respectively. The vacancy-compensated Sm^{2+} ions are thus seen to reequilibrate with respect to the vacancies within a fraction of a second at room temperatures after quenching from elevated temperatures. The fluorescence spectrum measured at cryogenic temperatures, therefore, should characterize the vacancy-compensated site distribution at some temperature somewhat lower than 300 K as sample preparation is made at room temperature, and rapid cooling for the sample to cryogenic temperatures is expected to freeze the distribution at some temperature below which the rate of vacancy reequilibration is negligibly small compared to the cooling rate.

We therefore attribute only the group-(a) lines

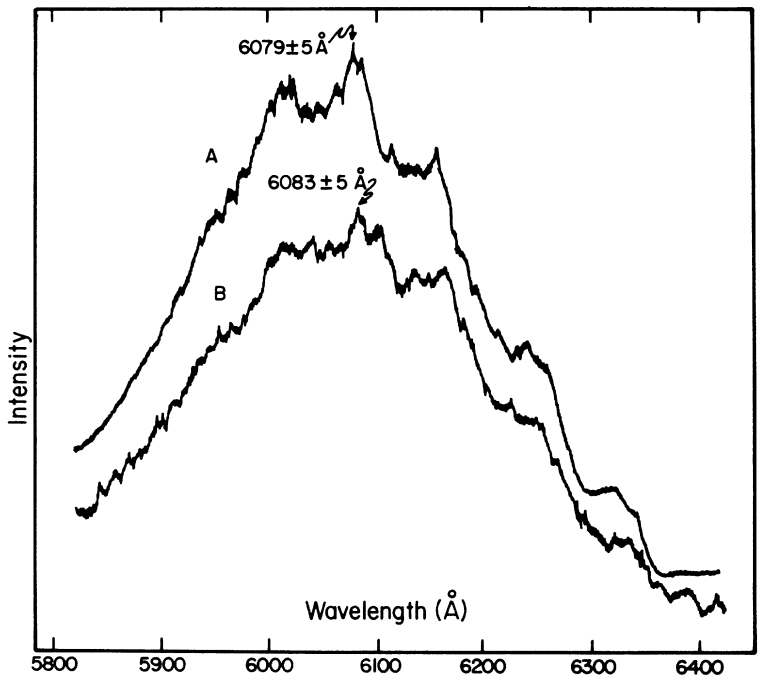

FIG. 7. 4.2-K excitation spectra of KCl : Sm^{2+} for two fluorescence lines at (a) 7014.7 Å ($^5D_0 \rightarrow {}^7F_1$) and (b) 7282.8 Å ($^5D_0 \rightarrow {}^7F_2$). The differences as well as the similarities in the structures of the two bands are to be noted.

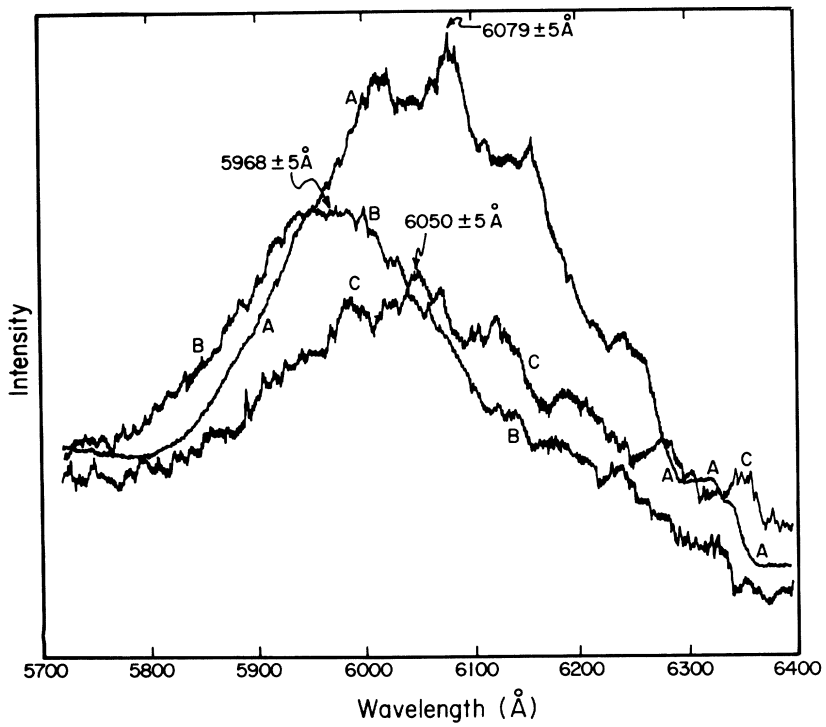

FIG. 8. 4.2-K excitation spectra of KCl : Sm^{2+} for three fluorescence lines at (a) 7014.7 Å ($^5D_0 \rightarrow {}^7F_1$), (b) 7022.7 Å ($^5D_0 \rightarrow {}^7F_1$), and (c) 7258.0 Å ($^5D_0 \rightarrow {}^7F_2$).

to $Sm^{2+} - K^+$ vacancy sites. The weak lines in groups (b) and (c) which disappear upon quenching from high temperatures cannot be attributed to the more distant, lower-symmetry $Sm^{2+} - K^+$ vacancy sites in view of Eq. (2) and the fact that, even if we were to ignore the implications of Eq. (2), the inten-

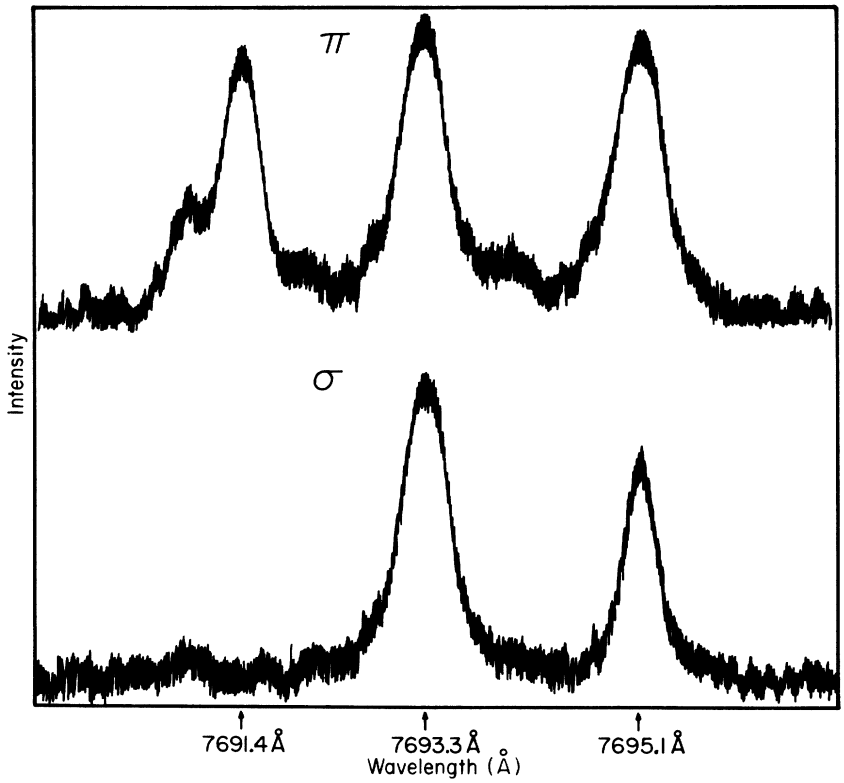

FIG. 9. Densitometer traces of the polarized Zeeman components of the $^5D_0 \rightarrow {}^7F_3$ 7693.5- and 7694.5-Å zero-field lines with $\vec{H}$ (46.6 kG) ∥ [100]. The 7691.4- and the 7695.1-Å components originate from the 7694.5-Å zero-field line while the 7693.3-Å line corresponds to the 7693.5-Å zero-field line.

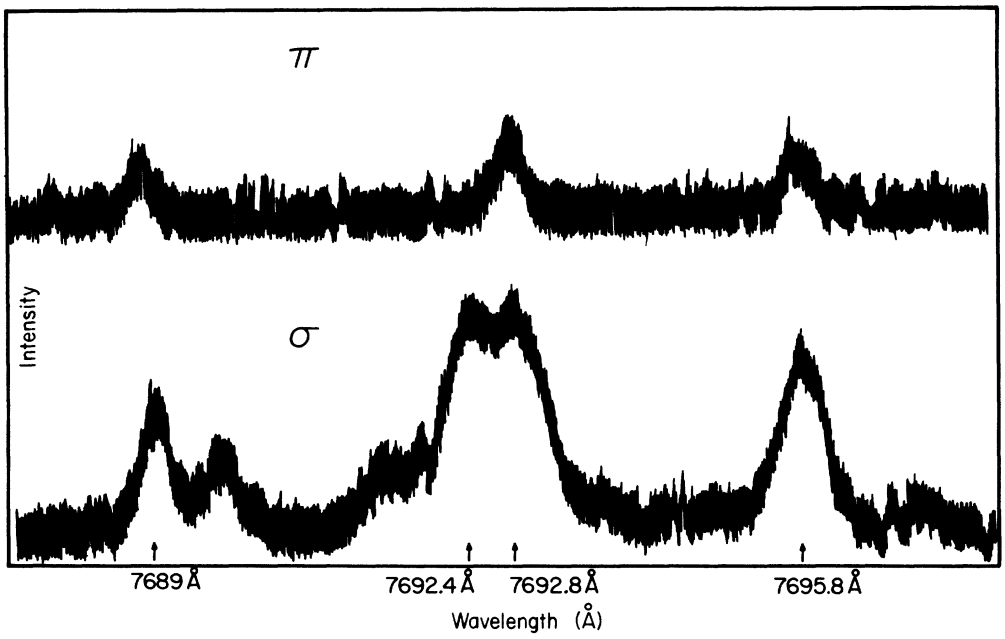

FIG. 10. Densitometer traces of the polarized Zeeman components of the $^5D_0 \rightarrow {}^7F_3$ 7693.5- and 7694.5-Å zero-field lines with $\vec{H}$ (93.5 kG) $\parallel$ [100]. The 7689.0- and 7695.8-Å components correspond to the 7694.5-Å zero-field line while the 7692.4- and 7692.8-Å components originate from the 7693.5-Å zero-field line.

sities of the lines arising from the distant sites are expected to increase rather than disappear at elevated temperatures.

The best symmetry assignments of the group-(a) lines are discussed here in the order of increasing J value of the $^5D_0 \rightarrow {}^7F_J$ transitions.

$$^5D_0 \rightarrow {}^7F_0$$

The single line at 6891.9 Å exhibits a blue shift of 0.25 cm^{-1} under a magnetic field of 93.5 kG, but no Zeeman splitting due to site inequivalence was observed.[40] From the polarization data presented by Bron and Heller,[31] this line can best be ascribed to the $C_{2v}A_1$ lower state. The lifetime 10.89 ± 0.06 msec observed for this line (Table I) is indistinguishable from those of the three prominent group-(a) lines in $^5D_0 \rightarrow {}^7F_1$ transitions (Table I), which are definitely of C_{2v} (1, 1, 0) site origin. (See discussion which immediately follows.)

$$^5D_0 \rightarrow {}^7F_1$$

The three lines at 7014.7, 7031.7, and 7048.2 Å are of C_{2v} origin. The representation origins of these three lines, as determined from Bron and Heller's polarization data[31] are B_1, A_2 or B_2, and B_2 or A_2, respectively, all of magnetic-dipole origin. These assignments are corroborated by the σ and π polarization data taken by Bradbury and Wong[45] under a magnetic field of 42 kG. The ZAF data of Fong and Bellows[40] indicate a well-resolved C_{2v} pattern arising from the 7014.7-Å line. Bradbury and Wong observed that the C_{2v} pattern should be inverted if the longer-wavelength component at 45°, 37.5°, and 52.5° observed by Fong and Bellows is absent. A reexamination of the original Fong-Bellows plates by the present authors show that while the presence of the very weak component in question is not mistaken, it probably originates from the weak zero-field line at 7015.3 Å (line VII of Fong and Bellows[40]). In the theoretical interpretation of Bradbury and Wong, the "S = 1" representation spin Hamiltonian (originally proposed by Fong and Wong[33] and further elaborated upon by Vredevoe, Chilver, and Fong[35]) was employed:

$$H_{eff} = g\mu_B \vec{H} \cdot \vec{S} + D[S_z^2 - \tfrac{1}{3}S(S+1)] + E(S_+^2 + S_-^2) . \tag{3}$$

With $g = 1.5$, $D = 0$, and $E = 34$ cm^{-1}, a fortuitous fit of the magnetic data was obtained.[45] Equation (3) actually corresponds to the perturbation Hamiltonian for the spherical basis states $|LSJM_J\rangle$ of the free Sm^{2+} ion:

$$H' = H_\mu + H_{cf} = g_\lambda \mu_B \vec{H} \cdot \vec{J} + \sum_{l,m,i} B_l^m Y_l^m(\theta_i, \phi_i), \tag{4}$$

where H_μ and H_{cf} are the magnetic and crystal field perturbation terms, respectively. The expansion coefficients B_l^m are determined by the position of the charge compensation in a given site

symmetry. The theoretical fit of the ZAF patterns can be achieved if a unique set of the parameters B_i^m can be obtained.

Equation (4) reduces to a form equivalent to Eq. (3) if only the $J=1$ manifold is considered. Bradbury and Wong's arbitrary choice of $D=0$, however, is inconsistent with the energy positions of the three Stark components in the $J=1$ manifold. With $B_2^0=84.1$ cm^{-1} and $B_2^2=85.3$ cm^{-1}, a good theoretical fit of the ZAF data was obtained [through the exact diagonalization of a 9×9 matrix using Eq. (4) and the $J=0$, 1, and 2 states] by Ford and Fong[51] for the three prominent $^5D_0 \rightarrow {}^7F_1$ lines, if the representation origins of the 7014.7-, 7031.7-, and 7048.2-Å lines are B_1, B_2, and A_2, respectively. This is in agreement with Bron and Heller's original assignment.

The same C_{2v} origin of the 7014.7-, 7031.7-, and 7048.2-Å lines is consistent with their respective lifetimes of 10.93 ± 0.04, 10.93 ± 0.11, and 10.83 ± 0.06 msec, which are indistinguishable within experimental error.

$$^5D_0 \rightarrow {}^7F_2$$

The characteristic lifetimes 10.83, 10.89 ± 0.09, and 10.89 ± 0.08 msec of the lines at 7264.4, 7304.6, and 7327.6 Å, respectively, indicate the C_{2v} origin of these three lines. This observation corroborates the well-resolved 93.5-kG C_{2v} ZAF pattern observed for the 7264.4-Å line by Fong and Bellows.[40] It is also consistent with the ZAF data obtained for the 7304.6-Å line which could be interpreted in terms of either an incomplete C_{2v} or C_{4v} ZAF pattern.

Of great interest is the zero-field line at 7282.8 Å for which apparently all the existing interpretations of data are in conflict. In the following, the experimental observations and conflicting interpretations are listed, and the correct assignment is deduced through a process of elimination.

(i) From polarized-excitation data, Bron and Heller[31] attributed the 7282.8-Å line to a magnetic-dipole transition, with the lower state being either A_2 or B_2 of the C_{2v} point group.

(ii) Fong and Bellows[40] attributed this line to a C_{4v}-site origin on account of the apparent ZAF pattern observed at 93.5 kG. The components of the pattern, however, were weak (as qualitatively indicated in Fig. 5 of Ref. 40 by the light lines drawn through the experimental points).

(iii) Bradbury and Wong[45] ruled out the C_{4v} origin and favored the C_{2v} interpretation from a consideration of the intensity of the Zeeman components with the fluorescence viewed parallel or perpendicular to the direction of the magnetic field $\vec{H}\parallel[100]$. However, Bradbury and Wong's polarization data cannot be interpreted in terms of the C_{2v} site symmetry if Bron and Heller's assignment of the magnetic dipole origin of this line was correct.

(iv) The characteristic lifetime 10.65 ± 0.03 msec of this line measured by the present authors definitely falls outside the experimental errors for the observed C_{2v} lifetime values (Table I), which rules out the C_{2v} origin [assuming that the C_{2v} (2, 2, 0) site, the fourth-nearest-neighbor pair, is statistically improbable[1]]. This, at first sight, supports the Fong-Bellows C_{4v} interpretation in view of (ii).

(v) The C_{4v} interpretation of this line, however, is not only in conflict with the intensity arguments as mentioned in (iii), but also with the present authors's observation that the two $\vec{H}\parallel[100]$ Zeeman components of a singlet C_{4v} transition must give rise to one σ and one π line[38]: Bradbury and Wong's

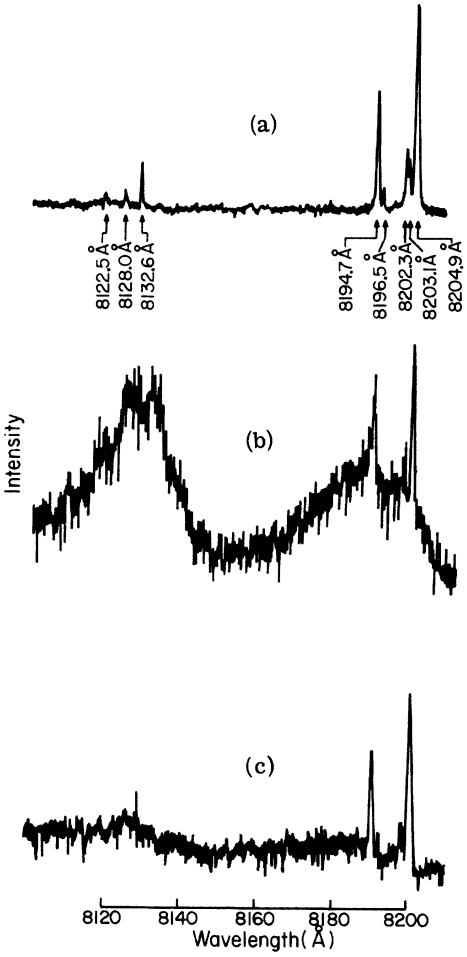

FIG. 11. The concentration dependence of KCl:Sm^{2+} fluorescence in the $^5D_0 \rightarrow {}^7F_4$ transition region: (a) 3.2×10^{18} cm^{-3}, (b) 3.5×10^{19} cm^{-3}, and (c) 5.1×10^{19} cm^{-3}. The experimental conditions employed for each measurement were identical with the exception of the full-scale chart-recorder sensitivity which was 5 V full scale for spectrum (a) and 2 V full scale for spectra (b) and (c).

polarization data show[45] that the long-wavelength component has both σ and π intensities, while the short-wavelength component gives only σ intensity.

(vi) The C_{2v}-origin interpretation is not only ruled out by (iii) and (iv), it is also inconsistent with the observed linewidths. The three prominent C_{2v} lines in the $^5D_0 \rightarrow {}^7F_1$ transitions show a monotonic increase in linewidth with increasing wavelength, as shown in Fig. 12. This behavior can be interpreted in terms of the phonon-assisted radiationless decay of the higher components of the Stark multiplet to lower crystal-field states. The problem of the radiationless decay of rare-earth Stark states and linewidths of radiative transitions has been explored experimentally by Yen, Scott, and Schawlow.[52] The rigorous theoretical treatment of phonon-assisted radiationless transitions in rare-earth ions has been given by Fong and Miller[53,54] in terms of quantum statistical correlation functions. If the 7282.8-Å line belongs to the C_{2v} Stark multiplet responsible for the 7264.4-, 7304.6-, and 7327.8-Å lines, its linewidth must be broadened (through radiationless decay to the lower state corresponding to the 7264.4-Å line) to the same extent as the $^5D_0 \rightarrow {}^7F_1$ 7031.7-Å line. The fact that the 7282.8-Å line is actually *narrower* than the 7264.4-Å line (see Fig. 12) rules out the possibility that these two lines are both of the same site origin.

If the 7282.8-Å line does not arise from either the C_{2v} or C_{4v} origin, it must originate from the C_s site. This process of elimination is based upon the assumption that only the $C_{2v}(1, 1, 0)$, $C_{4v}(2, 0, 0)$, and $C_s(2, 1, 1)$ vacancy-pair sites are important[1-6] and upon the conclusion that only vacancy-pair sites contribute to group-(a) lines. Experimental confirmation of the C_s assignment of the 7282.8-Å line given in terms of lifetimes and polarization data will be discussed in conjunction with the $^5D_0 \rightarrow {}^7F_3$ 7694.5-Å line.

The C_{2v} identification of the 7304.6- and 7327.6-Å lines by lifetimes represents the only positive confirmation of Bron and Heller's interpretation of their polarized-excitation experiments. On the basis of this confirmation, the 7304.6-Å line arises from an electric dipole transition with a lower-B_2 state according to Bron and Heller's interpretation, while the transition responsible for the 7327.6-Å

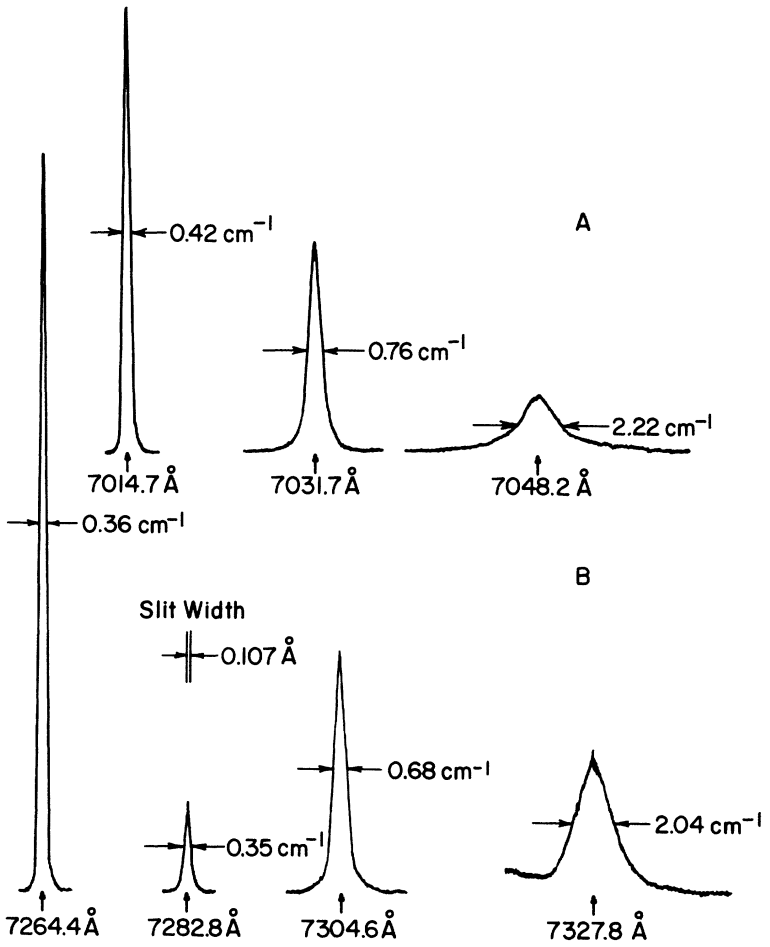

FIG. 12. A comparison of the linewidths of the three prominent KCl : Sm^{2+} $^5D_0 \rightarrow {}^7F_1$ lines with those of the four prominent $^5D_0 \rightarrow {}^7F_2$ lines. The linewidths measured at half-height are given in wave numbers.

line is an electric dipole with the lower state being either an A_1 or a B_1 representation.

Although Bradbury and Wong assigned the 7304.6-Å line to the C_{2v} origin, their polarization data can be interpreted in terms of either C_{2v} or C_{4v} site symmetry.[45] The speculative C_{2v} assignment of the broad line at 7327.8 Å by Bradbury and Wong on the basis of its being the last of the four observed allowed electric-dipole transitions is clearly inconsistent with the interpretations of Bron and Heller, who listed the missing line of their analysis as an electric dipole transition corresponding to an A_1 lower state.

$$^5D_0 \rightarrow {}^7F_3$$

The interpretation of the ZAF patterns [with the magnetic field rotated in the (001) plane] arising from the $^5D_0 \rightarrow {}^7F_3$ 7693.5- and 7694.5-Å lines by Bradbury and Wong[44] is compared with that by Fong, Sundberg, Heist, and Chilver[41] in Fig. 13. Three observations are made in the comparison.

(i) Although both zero-field lines at 7693.5 and 7694.5 Å are attributed to the same C_{2v} symmetry origin, approximately half of the observed points have not been accounted for in the Bradbury-Wong assignment [Fig. 13(a)]. A set of very weak lines to the long-wavelength side of 7694.5 Å is missing in the Bradbury-Wong plot.

(ii) The Bradbury-Wong C_{2v} assignment is based on the claim that the short-wavelength component of the 7694.5-Å zero-field line repels the 7693.5-Å line when the magnetic field is rotated away from the [100] direction. As "evidence" of this repulsion, it was noted[44] that the short-wavelength component of the 7694.5-Å line does not appear to be connected with the longer-wavelength line when the magnetic field is rotated by 90°. [See Fig. 13(a).] This observation is not corroborated by the data present in Fig. 13(b). It is not clear how such a repulsion is justified in terms of Bradbury and Wong's weak-field second-order theory. The Zeeman components of the 7694.5-Å line clearly do not interact with those of the 7693.5-Å line with $\vec{H} \| [100]$ (Fig. 2 of Ref. 41).

(iii) The 7694.5-Å line was attributed to the C_{2v} B_2 state by Bradbury and Wong on the basis of Zeeman-polarization data. This assignment is questionable: The longer-wavelength component should give a pure-σ polarization if the C_{2v} B_2 assignment is correct (see Table I of Ref. 44),

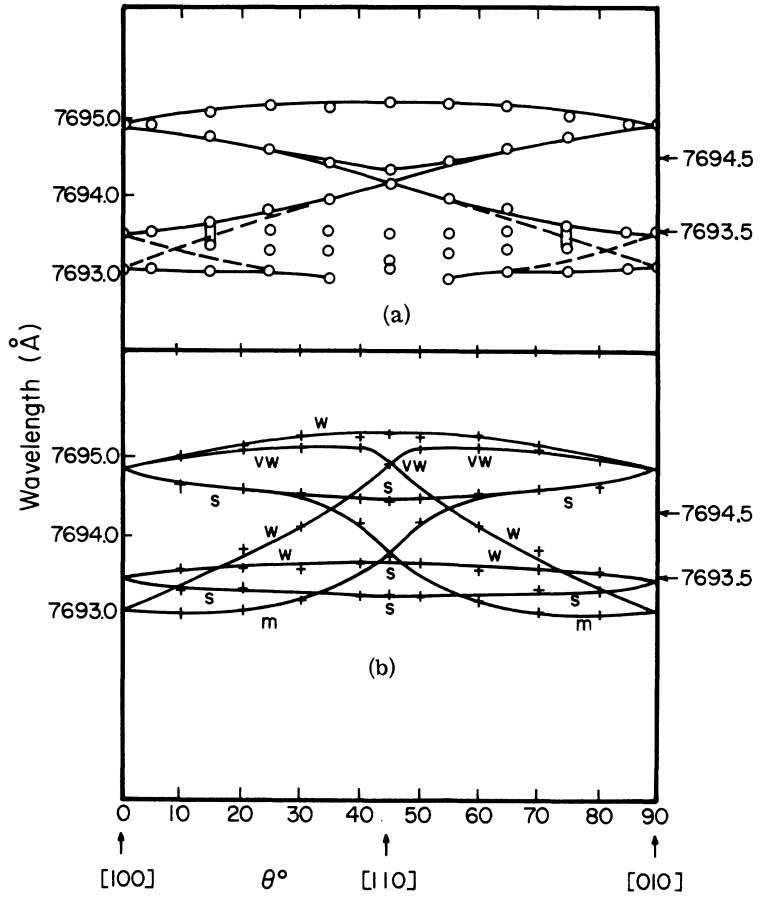

FIG. 13. Two conflicting interpretations of the 4.2-K 26.5-kG ZAF patterns with $\vec{H}$ rotated in the (001) plane observed for the $^5D_0 \rightarrow {}^7F_3$ zero-field lines (indicated by arrows) at 7693.5 and 7694.5 Å due to (a) Bradbury and Wong, (Ref. 44) and (b) Fong, Sundberg, Heist, and Chilver (Ref. 41).

while the experimental evidence of both Fig. 1(a) of Bradbury and Wong[44] and Fig. 9 of the present work clearly shows that the longer-wavelength component of the 7694.5-Å line gives both σ and π intensities.

The observation of two distinct lifetimes for the $^5D_0 \rightarrow {}^7F_3$ lines at 7693.5 Å (11.01 ± 0.08 msec) and 7694.5 Å (10.66 ± 0.17 msec) rules out the single C_{2v} site origin of these two lines and confirms the two-site interpretations of Fong, Sundberg, Heist, and Chilver[41] [Fig. 10(b)]. The C_s origin of the 7694.5-Å line is thus confirmed. The 7693.5-Å line is most probably of C_{2v} origin, its lifetime being indistinguishable from the C_{2v} lifetimes. The C_{2v} origin of the 7693.5-Å line is consistent with the apparent C_{3v} ZAF pattern shown in Fig. 1(b) since the missing components could be easily obscured by the large density of lines in the vicinity of 7693.5 Å [see Fig. 1(b) and Fig. 3 of Ref. 41].

As confirmation of the C_s assignment of the 7694.5- and 7282.8-Å lines, we have made analysis of the polarization properties of the Zeeman components of a C_s zero-field line under a magnetic field $\vec{H} \| [100]$. The x, y, and z coordinates of the $C_s(2, 1, 1)$ site are shown in Fig. 14. The axis containing the Sm^{2+} ion and the K^+ vacancy is taken to be the x axis. The axis normal to the reflection plane is chosen as the z axis. The y axis is thus defined within the framework of the right-handed coordinate system. The projections of the x, y, and z axes of the 12 magnetically distinguishable sites on the [100] and [001] axes of the KCl lattice, as well as the relative π and σ polarized intensities $I(\pi)$ and $I(\sigma)$ for electric dipole transitions when the fluorescence is viewed along [010] with $\vec{H} \| [100]$, are listed in Table II. If the transition is $A' \rightarrow A'$, the component due to sites $c, c', d, d', e, e', f, f'$ with $\vec{H} \| [100]$ will show σ and π polarizations with $I(\sigma) = 1.5\, I(\pi)$, while the component due to sites a, a', b, b' will show σ and π polarizations with $I(\sigma) = 0.5\, I(\pi)$. If the transition is $A' \rightarrow A''$, the component due to sites $c, c', d, d', e, e', f, f'$ will still have nonvanishing intensities for both σ and π polarizations, while the component due to sites a, a', b, b' will be pure-σ polarized. For magnetic dipole transitions, interchange A' and A'' and exchange σ and π as found in Table II. At high fields, the A' and A'' states will be admixed, and both Zeeman components will give $\sigma\pi$ polarization. The polarization data presented in Figs. 9 and 10 of the present work and Fig. 4 of Ref. 45 are in excellent agreement with theory if the 7694.5- and 7282.8-Å lines are attributed to the $A' \rightarrow A'$ magnetic dipole and $A' \rightarrow A''$ electric dipole transitions, respectively, giving strong confirmation to the C_s assignment of these two zero-field lines.

The 7693.5-Å line is assigned C_{2v} on the basis of its characteristic lifetime. This is consistent with the fact that all group-(a) lines originate from $Sm^{2+} - K^+$ vacancy sites even though the ZAF pattern is apparently C_{3v} [Fig. 12(b)]. (The C_{3v} ZAF pattern can only be attributed to an O^{2-} compensated site. The role of O^{2-} compensation is discussed in Sec. VII.) The splitting of this line at fields $\gtrsim 60$ kG gives rise to a $\sigma\pi$ component at longer wavelength and a σ component at shorter wavelength (Fig. 10). This is consistent with the C_{2v} description of an electric dipole transition with an A_1 or B_1 lower state according to Table V of Ref. 45.

$$^5D_0 \rightarrow {}^7F_4$$

Of the four group-(a) lines in this transition region, the 8204.9-Å line is clearly of C_{2v} origin, its lifetime 11.01 ± 0.11 msec being indistinguishable from the C_{2v} lifetimes observed for the lower-J transitions. The longer-wavelength component of the two Zeeman components with $\vec{H} \| [100]$ has equal σ and π polarization,[38,55] a situation similar to that observed for the $^5D_0 \rightarrow {}^7F_3$ 7693.5-Å line. Accordingly, the 8204.9-Å line is attributed to an electric dipole transition with either an A_1 or B_1 lower state.

The 8132.6- and 8194.7-Å lines give rise to well-resolved C_{4v} ZAF patterns. Their lifetimes, 10.54 ± 0.16 and 10.51 msec, respectively, distinctly fall outside the range of the averaged C_{2v} lifetime 10.92 ± 0.09 msec, which gives definitive support to the C_{4v} interpretation. On the basis of the polarization data of Fong and Bellows,[38,55] the 8132.6-Å line can be uniquely attributed to a magnetic dipole transition with an A_2 lower state. The

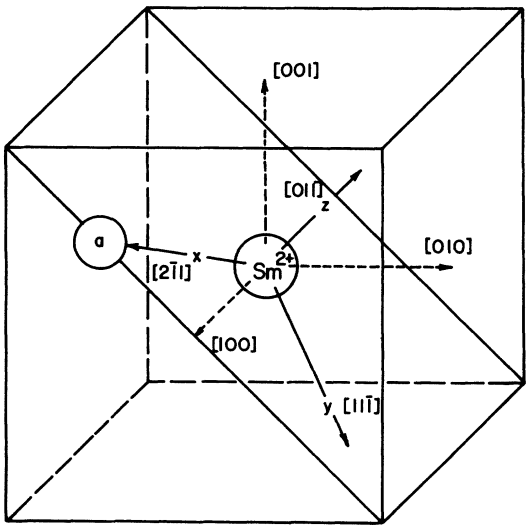

FIG. 14. A diagramatic representation of the local xyz coordinate axes for the $C_s(2, \bar{1}, 1)$ $Sm^{2+}-K^+$ vacancy pair. The notation a designates the K^+ vacancy position.

full C_{4v} ZAF pattern arising from the 8194.7-Å line can be attributed to an E representation or an "accidental" degeneracy of two states of A_1 and A_2 representations. A discussion of the cause of such an accidental degeneracy has been given by Fong and Bellows.[38]

We believe Bradbury and Wong's assignment[46] of the 8132.6- and 8194.7-Å lines to the $C_{2v}(1,1,0)$ site to be wrong: From second-order perturbation theory, these authors demonstrated that for C_{2v}, a two-level system involving an A_1 and B_1 combination "will give exactly the same first-order Zeeman-effect pattern as the C_{4v} symmetry."[45] These authors surmised[46] that such is indeed the case for the zero-field line at 8194.7 Å, "except that variation is quadratic in $H_0\cos\theta$ {where θ is the angle between $\vec{H}$ and the [100] axis in the (001) plane} instead of linear,"[45] which is clearly shown to be false in the comparison of the linear fit of the $\vec{H}\parallel[100]$ field-dependence data of the 8194.7-Å line with the hypothetical quadratic dependence of Bradbury and Wong's second-order theory (Fig. 15).

$$^5D_0 \rightarrow {}^7F_5$$

Other than the C_{2v} assignment of the 8746.4- and 8747.3-Å lines by Fong and Wong,[33] no definite symmetry assignments are available for the group-(a) $^5D_0 - {}^7F_5$ lines. The tentative C_s assignment of the 8778.4-Å line by Fong[37] must await confir-

TABLE II. The projections of the x, y, and z components of each of the 12 magnetically distinguishable C_s sites on the [100] and [001] axes. The weak-field π and σ intensities for an electric dipole transition to an A' or A'' lower state are deduced on the basis that the magnetic field $\vec{H}$ is parallel to [100] and the fluorescence is viewed in the [010] direction. The corresponding π and σ intensities for a magnetic dipole transition are obtained by interchanging A' and A'' and exchanging π with σ.

	Site axes			Projection on the [100] axis, parallel to the magnetic field (π polarization)			Projection on the [001] axis, perpendicular to the magnetic field (σ polarization)		
Site	x	y	z	x	y	z	x	y	z
a	$[2\bar{1}1]$	$[11\bar{1}]$	[011]	$\frac{2}{\sqrt{6}}$	$\frac{1}{\sqrt{3}}$	0	$\frac{1}{\sqrt{6}}$	$-\frac{1}{\sqrt{3}}$	$\frac{1}{\sqrt{2}}$
a'	$[2\bar{1}\bar{1}]$	[111]	$[0\bar{1}1]$	$\frac{2}{\sqrt{6}}$	$\frac{1}{\sqrt{3}}$	0	$-\frac{1}{\sqrt{6}}$	$\frac{1}{\sqrt{3}}$	$\frac{1}{\sqrt{2}}$
b	[211]	$[1\bar{1}\bar{1}]$	$[01\bar{1}]$	$\frac{2}{\sqrt{6}}$	$\frac{1}{\sqrt{3}}$	0	$\frac{1}{\sqrt{6}}$	$-\frac{1}{\sqrt{3}}$	$-\frac{1}{\sqrt{2}}$
b'	$[21\bar{1}]$	$[1\bar{1}1]$	$[0\bar{1}\bar{1}]$	$\frac{2}{\sqrt{6}}$	$\frac{1}{\sqrt{3}}$	0	$-\frac{1}{\sqrt{6}}$	$\frac{1}{\sqrt{3}}$	$-\frac{1}{\sqrt{2}}$
c	[121]	$[\bar{1}1\bar{1}]$	$[\bar{1}01]$	$\frac{1}{\sqrt{6}}$	$-\frac{1}{\sqrt{3}}$	$-\frac{1}{\sqrt{2}}$	$\frac{1}{\sqrt{6}}$	$-\frac{1}{\sqrt{3}}$	$\frac{1}{\sqrt{2}}$
c'	$[12\bar{1}]$	$[\bar{1}11]$	[101]	$\frac{1}{\sqrt{6}}$	$-\frac{1}{\sqrt{3}}$	$\frac{1}{\sqrt{2}}$	$-\frac{1}{\sqrt{6}}$	$\frac{1}{\sqrt{3}}$	$\frac{1}{\sqrt{2}}$
d	$[\bar{1}21]$	$[11\bar{1}]$	$[\bar{1}0\bar{1}]$	$-\frac{1}{\sqrt{6}}$	$\frac{1}{\sqrt{3}}$	$-\frac{1}{\sqrt{2}}$	$\frac{1}{\sqrt{6}}$	$-\frac{1}{\sqrt{3}}$	$-\frac{1}{\sqrt{2}}$
d'	$[\bar{1}2\bar{1}]$	[111]	$[10\bar{1}]$	$-\frac{1}{\sqrt{6}}$	$\frac{1}{\sqrt{3}}$	$\frac{1}{\sqrt{2}}$	$-\frac{1}{\sqrt{6}}$	$\frac{1}{\sqrt{3}}$	$-\frac{1}{\sqrt{2}}$
e	[112]	$[\bar{1}\bar{1}1]$	$[1\bar{1}0]$	$\frac{1}{\sqrt{6}}$	$-\frac{1}{\sqrt{3}}$	$\frac{1}{\sqrt{2}}$	$\frac{2}{\sqrt{3}}$	$\frac{1}{\sqrt{3}}$	0
e'	$[1\bar{1}2]$	[111]	$[\bar{1}10]$	$-\frac{1}{\sqrt{6}}$	$\frac{1}{\sqrt{3}}$	$-\frac{1}{\sqrt{2}}$	$\frac{2}{\sqrt{6}}$	$\frac{1}{\sqrt{3}}$	0
f	$[1\bar{1}2]$	$[\bar{1}11]$	$[\bar{1}\bar{1}0]$	$\frac{1}{\sqrt{6}}$	$-\frac{1}{\sqrt{3}}$	$-\frac{1}{\sqrt{2}}$	$\frac{2}{\sqrt{6}}$	$\frac{1}{\sqrt{3}}$	0
f'	$[\bar{1}12]$	$[1\bar{1}1]$	[110]	$-\frac{1}{\sqrt{6}}$	$\frac{1}{\sqrt{3}}$	$\frac{1}{\sqrt{2}}$	$\frac{2}{\sqrt{6}}$	$\frac{1}{\sqrt{3}}$	0

Sites	Relative polarized intensities		
a, a', b, b'	$I\pi$	$\frac{A'}{4}$	$\frac{A''}{0}$
	$I\sigma$	2	2
$c, c', d, d', e, e', f, f'$	$I\pi$	$\frac{A'}{4}$	$\frac{A''}{4}$
	$I\sigma$	6	2

mation in view of the lack of resolution.

$^5D_0 \rightarrow {}^7F_6$

Excluding the hypothetical "C_{2v} two-level-system psuedo-C_{4v} ZAF pattern" proposed by Bradbury and Wong, the definitive C_{4v} pattern observed by Fong and Wong[33] for the pair of lines at 9439.1 and 9440.0 Å [which are, by far, the most intense of the group-(a) lines (see Table I)] cannot be interpreted in terms of any other symmetry origin. The splitting pattern, as well as the polarization data, can be readily accounted for in terms of the $C_{4v}(2, 0, 0)$ site.[33] Bradbury and Wong[46] found it "puzzling why Fong and Wong persist in calling these lines C_{4v} when they (Fong and Wong) invoke a C_{2v} spin Hamiltonian to account for the separation of the lines at zero field." The Hamiltonian employed by Fong and Wong[33] is a C_{4v} fictitious Hamiltonian in the $S = 1$ representation.[35] A small nonaxial perturbation term was included to induce a zero-field splitting of the fictitious E representation (which could actually be a pair of A_1 and A_2 states). The angular-dependence calculation of the position variation of the Zeeman components was based on the geometry of a C_{4v} $Sm^{2+} - K^+$ vacancy pair, and the treatment was a uniquely C_{4v} situation. Bradbury and Wong have confused the use of a fictitious Hamiltonian such as Eq. (3) with that of a realistic Hamiltonian such as Eq. (4).

Characteristic Lifetimes of $C_{2v}(1,1,0)$ $C_{4v}(2,0,0)$, and $C_s(2,1,1)$ Sites

The best assignments of symmetry origins for 17 prominent lines are listed in Table I. The average and standard deviation ($N = 27$) for all the lifetime determinations of $C_{2v}(1, 1, 0)$ lines is 10.92 ± 0.09 msec. The average and standard deviation ($N = 5$) for all the lifetime determinations of the $C_{4v}(2, 0, 0)$ lines is 10.53 ± 0.14 msec. The average and standard deviation ($N = 6$) for all the lifetime determinations of the $C_s(2, 1, 1)$ lines is 10.65 ± 0.13 msec.

The data on the temperature-dependent quenching of KCl : Sm^{2+} fluorescence of the present work are in agreement with Bradbury and Wong's data. The group-(a) lines of the present work correspond to the α lines of Bradbury and Wong, and the group-(b) and -(c) lines observed by the present authors correspond to Bradbury and Wong's lines which were not resolved by those authors because of the limited temperature range of their experiments. The temperature dependence of δ and ϵ of Bradbury and Wong is indistinguishable from that of group (b). The β lines, which are substantially quenched at 4.2 K, are not observed in the present work except for the 6899.1-Å line. The lifetime of the 6899.1-Å line is < 50 μsec (Table I).

Only one 4.2-K lifetime, 9.8 msec, was reported

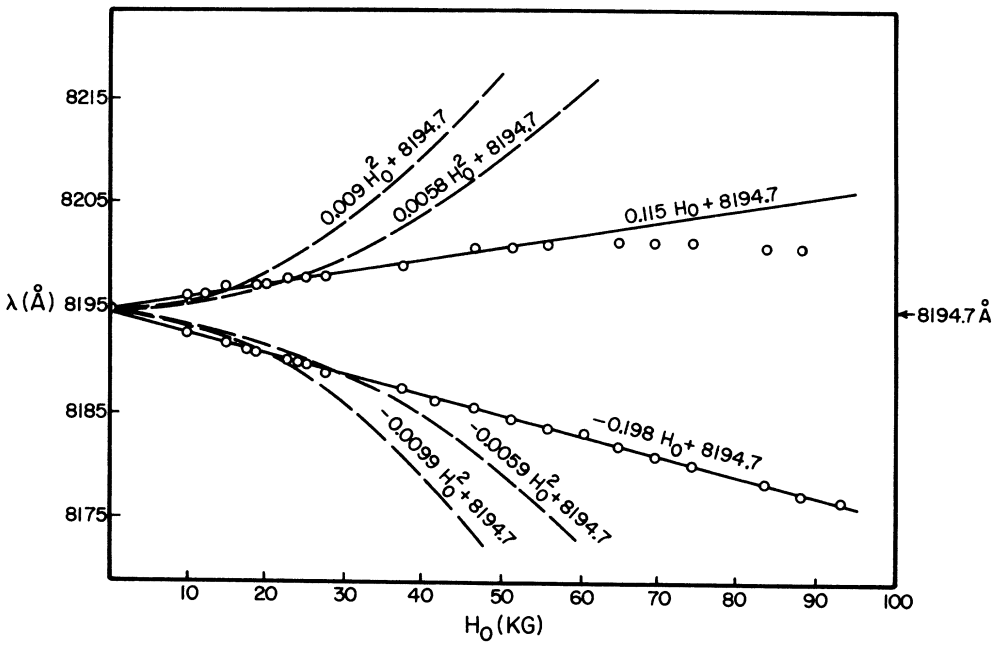

FIG. 15. A comparison of the linear fit of the field-dependence data for the $^5D_0 \rightarrow {}^7F_4$ 8194.7-Å line with examples of the hypothetical quadratic dependence of Bradbury and Wong's second-order theory. The sublinear field dependence of the longer-wavelength component is due to repulsion through interaction with a nearby crystal state. The equations for the four hypothetical quadratic field dependences represent the best fits at low-field strengths.

by Bradbury and Wong[46] for the prominent group-(a) lines. No lifetimes were reported by these authors on the weaker lines in groups (b), (c), and β. The 4.2-K lifetime, 9.8 msec, is more than 10% lower than the characteristic C_{2v} lifetime 10.92 ± 0.09 msec reported in the present work. The lifetime value 11.5 ± 1 msec measured for $^5D_0 - {}^7F_0$ by Baldini, Cartoceti, and Guzzi,[42] on the other hand, is in agreement, although their large experimental uncertainties are typical of lifetime work without proper signal averaging. Since no standard deviations were given for any of Bradbury and Wong's lifetime measurements, there is no way to check the reproducibility of their experiments.

VII. ORIGINS OF THE WEAK LINES IN GROUPS (b) and (c)

The experiments dealing with the quenching of group-(b), -(c), and -β lines after high-temperature annealing (Fig. 4) reproduce the observations of earlier investigators,[25,26,31] who attributed the phenomenon to the dispersion of clusters of $Sm^{2+}-K^+$ vacancy pairs, and, to a perhaps lesser extent, $Sm^{2+}-O^{2-}$ complexes. The subsequent reappearance of these lines when the samples are stored at room temperature corresponds to the phenomenon of "dipole decay" observed by Dryden and coworkers[20-22] when alkali halides doped with Pb^{2+} and Mn^{2+} ions are quenched to room temperature from ~ 773 K. Isolated ion-defect pairs possess electric dipole moments. When the dipolar pairs aggregate to form clusters at sufficiently low temperatures, the total dipole moment of the crystal decreases. The dipole decay rate is thus a measure of the rate of cluster formation. The role of O^{2-} compensation is demonstrated in the observation of the cubic Sm^{2+} site in quenched crystals in which O^{2-} ions have been intentionally introduced.[26]

The problem of cluster formation in $KCl:Sr^{2+}$ has been treated theoretically by Naberhuis and Fong.[6] Numerical calculations have been made by assuming the principle of linear superposition. These calculations show that while extensive dimer formation occurs through wide ranges of temperatures and concentrations, trimer and higher cluster formations become important at concentrations $> 10^{19}$ cm^{-3}. At 300 K, the probability of a Sm^{2+} ion occurring in a dimeric cluster of two $Sm^{2+}-K^+$ vacancy pairs is approximately 36% at 10^{18} cm^{-3}, assuming no trimerization. This is in qualitative agreement with the relative total intensity of the group-(a) lines compared with that of the group-(b), -(c), and -β lines reported by Bradbury and Wong[46] if we assume that the dimeric cluster is the origin of the weak lines in groups (b), (c), and β. At higher concentrations, clusters higher than the dimers will form. In $KCl:Sm^{2+}$, the formation of higher clusters is reflected in the appearance of new lines and bands as reported by Fong, Heist, Chilver, Bellows, and Ford.[36] The photomultiplier traces (measured by the present authors) of the $^5D_0 - {}^7F_4$ fluorescence for the three samples with concentrations 3.2×10^{18}, 3.5×10^{19}, and 5.1×10^{19} Sm^{2+}-ions cm^{-3}, respectively, are shown in Fig. 11. Figures 11(a) and 11(b) correspond to Bradbury and Wong's type-I and type-II spectra (Fig. 3 of Ref. 46), respectively, while Bradbury and Wong's type-I spectrum and the spectrum in Fig. 11(a) are *identical* to the original Fong and Wong spectrum displayed in Fig. 5(a) of Ref. 33.

The ratio $\eta > 3$ for the normalized intensities of the groups (b), (c), and β lines in the so-called type-I crystals to those in the type-II crystals observed by Bradbury and Wong is interesting. It means that, according to the theoretical interpretations of Naberhuis and Fong,[6] at higher concentrations the dimeric clusters become less populated than higher clusters, whose presence is reflected by the "new" line and broad-band fluorescence shown in Figs. 11(b) and 11(c), as well as the so-called type-II spectrum. It is clear from Fig. 11 that actually the intensity of the group-(a) lines is also "quenched" as the dopant concentration increases. A more detailed study on the effect of rare-earth-ion concentration on fluorescence in terms of the phenomena of cluster formation and concentration quenching of fluorescence intensities will be reported elsewhere.[56]

VIII. CONCLUDING REMARKS

The experimental results, interpretations, and symmetry assignments are summarized in Table I. The concept of *types* of divalent-cation sites (such as single vacancy pairs, dimeric clusters, and O^{2-} compensated sites), which has become prominent among workers in the defect crystalline state in recent years, is seen to play an important role in the present work. The similarities in the lifetimes, quenching behavior, and excitation spectra of the various $Sm^{2+}-K^+$ vacancy pairs raise an interesting question as to the nature of the excitation process. An answer to this question is attempted by Fong[57] in a theoretical treatment of the radiationless quenching process by time-correlation functions in the adiabatic approximation. The rapid relaxation of site β (Table I) deserves further investigation.

In view of the peculiar optical properties of the Sm^{2+} ion, $KCl:Sm^{2+}$ serves as an important example of the compensated lattice. Bradbury and Wong correctly stated that any attempt to utilize the fluorescent spectrum in determining the site distributions must start with the correct identification of the fluorescence lines. Most of the spectroscopic interpretations, however, are usually

ambiguous. It is only through the confirmation of a number of *different* spectroscopic analyses that conclusions can be made with any degree of confidence. These conclusions then become amenable to further interpretation in the light of the available background knowledge of the sample crystal. Such background knowledge includes the dopant concentration, history of heat treatment, ion and defect mobilities, binding energies of ion and defect pairs, as well as other aspects of the defect crystalline state embodied in more than three decades of the literature since the early investigations of Koch and Wagner.[58] The importance of the above consideration is demonstrated in the present controversy. The distribution theory of Fong and co-workers[1-6] is constructed on the basis of well-established theoretical and experimental results.[7-30] Without proper consideration of the concentrations of the sample crystals and the many well-established facts such as binding energies[1,3-5,18,19,27-30] and mobilities[15,18,19,20-22,26,50] of ions and defects, Bradbury and Wong dismissed the distribution theory on the basis of either "wrong binding energies" or the lack of correlation between the theoretical populations and the spectrum because the Sm^{2+}–K^{+} vacancy system does not reach thermodynamic equilibrium at room temperature, at least in "a couple of years." To substantiate this point, Bradbury and Wong presented plausible spectroscopic arguments with neither the necessary experimental techniques [such as signal averaging and high-magnetic fields (Sec. IV)] nor the self-consistency in the proof of their theoretical postulates [such as the pseudo-C_{4v} second-order C_{2v} ZAF patterns (Sec. VI) and the C_{2v} assignment of the $^5D_0$–$^7F_3$ lines (Sec. VI)]. It is clear that the principles of optical spectroscopy are not only limited in usefulness in the study of compensated lattices, but can also prove to be extremely misleading when their application is made on the basis of inadequate experiments and in the light of erroneous preconceived notions. Of the spectroscopic methods employed in the present work, the ZAF technique gives the most unambiguous handle on the problem of site symmetry in compensated lattices. All the symmetry-origin assignments determined previously on complete ZAF patterns are confirmed by the supporting data on lifetime measurements, polarization, and excitation spectra. While the theoretical fit of the experimental ZAF data employing the Hamiltonian in Eq. (4) is a laborious task in numerical analysis, Ford and Fong[51] have, on the basis of the analysis of the present work, carried out a satisfactory calculation of all the observed C_{2v} ZAF patterns by the diagonalization of 9×9 matrices using Eq. (4) and the Stark states in the $J=0$, 1, and 2 manifolds.

The real strength of the ZAF technique as an analytical tool in symmetry determination lies in the fact that it is possible to identify experimental ZAF patterns according to the schematic patterns given by Fong, Sundberg, Heist, and Chilver.[41] When the Zeeman components are not well resolved or when the patterns are incomplete, it is necessary to confirm the ZAF determination by supporting data such as characteristic lifetimes and polarizations of the ZAF components. Bradbury and Wong's pseudo-C_{4v} second-order C_{2v} patterns invoking two levels are expected to be highly unlikely when the Stark states of the $4f^n$ configuration are involved: Typical observed Zeeman splittings in well-resolved patterns fall in the range 10–60 cm^{-1}, while typical energy separations between the crystal Stark states of the Sm^{2+} ion in KCl are on the order of 30 cm^{-1} (e.g., the C_{2v} Stark components in $J=1$, and 2). The analysis of the 8194.7-Å ZAF pattern on the basis of the two-level pseudo-C_{4v} argument by Bradbury and Wong has been shown to be incorrect (Sec. VI, Fig. 15).

The lifetime measurements, when proper signal averaging is available, are important as confirmation data on the ZAF symmetry determinations. Radiationless-quenching, polarization, and excitation-spectroscopic data are only useful as supporting data when accurate lifetime measurements and ZAF data are available.

ACKNOWLEDGMENTS

We are grateful to S. L. Naberhuis for the expert help in setting up the necessary computer programs employed in the lifetime experiments. The high-field-polarization data were taken by J. C. Bellows at the Francis Bitter National Magnet Laboratory.

---

*Research supported under the sponsorship of the Advanced Research Projects Agency Grant No. SD102.

†Paper part of work submitted by R. H. Heist and C. R. Chilver to the Graduate School of Purdue University in partial fulfillment of the requirement for the degree of Doctor of Philosophy.

‡Present address, Department of Chemistry, University of California, Los Angeles, Calif. 90024.

§To whom reprint requests should be addressed.

[1] F. K. Fong, Phys. Rev. 187, 1009 (1969).

[2] R. H. Heist and F. K. Fong, Phys. Rev. B 1, 2970 (1970).

[3] F. K. Fong, R. L. Ford, and R. H. Heist, Phys. Rev. B 2, 4202 (1970).

[4] R. L. Ford and F. K. Fong, J. Chem. Phys. 55, 2532 (1971).

[5] F. K. Fong, in *Solid State Electrochemistry*, edited by J. Hladik (Academic, London, 1972), Chap. 3, pp.

79–126.
[6]S. L. Naberhuis and F. K. Fong, J. Chem. Phys. 55, 1174 (1972).
[7]R. G. Breckenridge, J. Chem. Phys. 16, 959 (1948).
[8]R. G. Breckenridge, J. Chem. Phys. 18, 913 (1949).
[9]A. B. Lidiard, in *Report on the Conference on Defects in Crystalline Solids* (The Physical Society, London, 1954), p. 283.
[10]Y. Haven and J. H. van Santen, J. Chem. Phys. 22, 1146 (1954).
[11]Y. Haven and J. H. van Santen, Suppl. Nuovo Cimento 7, 605 (1958).
[12]A. D. Franklin, J. Res. Natl. Bur. Std. 67A, 291 (1963).
[13]A. D. Franklin, A. Shorb, and J. B. Wachtman, Jr., J. Res. Natl. Bur. Std. 68A, 425 (1964).
[14]A. B. Lidiard, Phys. Rev. 94, 29 (1954).
[15]A. B. Lidiard, in *Handbuch der Physik*, edited by S. Flügge (Springer-Verlag, Berlin, 1957), Vol. XX, Pt. 2, pp. 246–349.
[16]H. W. Etzel and R. J. Mauer, J. Chem. Phys. 18, 1003 (1950).
[17]R. G. Fuller, C. L. Marguardt, M. H. Reilly, and John C. Wells, Jr., Phys. Rev. 176, 1036 (1968).
[18]G. D. Watkins, Phys. Rev. 113, 79 (1959).
[19]G. D. Watkins, Phys. Rev. 113, 91 (1959).
[20]J. S. Cook and J. S. Dryden, Australian J. Phys. 13, 260 (1960).
[21]J. S. Cook and J. S. Dryden, Proc. Phys. Soc. (London) 80, 479 (1962).
[22]J. S. Dryden and G. G. Harvey, J. Phys. C 2, 603 (1969).
[23]R. Capelletti and E. DeBenedetti, Phys. Rev. 165, 981 (1968).
[24]K. Srivastava, Nuovo Cimento 47B, 251 (1967).
[25]E. Patscheke, Z. Physik 186, 63 (1965).
[26]J. B. Fenn, Jr., D. Cox, and F. K. Fong, J. Chem. Phys. 56, 188 (1972).
[27]J. R. Reitz and J. L. Gammel, J. Chem. Phys. 19, 894 (1951).
[28]F. Bassani and F. G. Fumi, Nuovo Cimento 11, 274 (1954).
[29]M. P. Tosi and G. A. Airoldi, Nuovo Cimento 8, 584 (1958).
[30]P. Brauer, Z. Naturforsch. 6a, 255 (1951).
[31]W. E. Bron and W. R. Heller, Phys. Rev. 136, A1433 (1964).
[32]F. K. Fong and E. Y. Wong, *Proceedings on Conference on Optical Properties of Crystals* (Wiley, New York, 1967), p. 137.
[33]F. K. Fong and E. Y. Wong, Phys. Rev. 162, 348 (1967).
[34]M. Buchanan and E. J. Woll, Jr., Can. J. Phys. 47, 1757 (1969).
[35]L. A. Vredevoe, C. R. Chilver, and F. K. Fong, *Progress in Solid State Chemistry*, edited by H. Reiss (Pergamon, New York, 1970), Vol. V, Chap. 6, pp. 399–463.
[36]F. K. Fong, R. H. Heist, C. R. Chilver, J. C. Bellows, and R. L. Ford, J. Luminescence 2, 823 (1970).
[37]F. K. Fong, Phys. Rev. B 1, 4157 (1970).
[38]F. K. Fong and J. C. Bellows, Phys. Rev. B 1, 4240 (1970).
[39]C. R. Chilver and F. K. Fong, Chem. Phys. Letters 7, 229 (1970).
[40]F. K. Fong and J. C. Bellows, Phys. Rev. B 1, 2636 (1970).
[41]F. K. Fong, M. N. Sundberg, R. H. Heist, and C. R. Chilver, Phys. Rev. B 3, 50 (1971).
[42]G. Baldini, M. Cartoceti, and M. Guzzi, Solid State Commun. 8, 1697 (1970).
[43]R. E. Bradbury, Ph. D. thesis (University of California at Los Angeles, California, 1971) (unpublished).
[44]R. E. Bradbury and E. Y. Wong, Phys. Rev. B 4, 690 (1971).
[45]R. E. Bradbury and E. Y. Wong, Phys. Rev. B 4, 694 (1971).
[46]R. E. Bradbury and E. Y. Wong, Phys. Rev. B 4, 702 (1971).
[47]L. Pauling, *Nature of the Chemical Bond* (Cornell U. P., Ithaca, New York, 1960).
[48]F. K. Fong, J. A. Cape, and E. Y. Wong, Phys. Rev. 151, 299 (1966).
[49]B. Welber and E. E. Tynan, Rev. Sci. Instr. 38, 137 (1967).
[50]R. W. Dreyfus and A. S. Nowick, J. Appl. Phys. 33, 473 (1962).
[51]R. L. Ford and F. K. Fong, J. Chem. Phys. 56, 1972 (1972).
[52]W. M. Yen, W. C. Scott, and A. L. Schawlow, Phys. Rev. 136, A271 (1964).
[53]F. K. Fong and M. M. Miller, Chem. Phys. Letters 10, 408 (1972).
[54]F. K. Fong, S. L. Naberhuis, and M. M. Miller, J. Chem. Phys. (to be published).
[55]Bradbury and Wong (Ref. 45) were correct in pointing out the possibility of analyzer mislabeling in the polarization work of Fong and Bellows (Ref. 38). A double check by H. V. Lauer and M. N. Sundberg at Purdue indicates that the σ and π designations in Fig. 1 of Ref. 38 should be reversed. The σ and π designations for the zero-field line at 8132.6 Å are correct.
[56]J. B. Fenn, Jr., J. C. Wright, and F. K. Fong, J. Chem. Phys. (to be published).
[57]F. K. Fong, J. Chem. Phys. (to be published).
[58]E. Koch and C. Wagner, Z. Physik. Chem. B38, 295 (1937).